Preprints of the 19th World Congress
The International Federation of Automatic Control
Cape Town, South Africa. August 24-29, 2014

Nonlinear optimal wave energy converter control with application to a flap-type device ⋆

Giorgio Bacelli * **John V. Ringwood** **

* *Center for Ocean Energy Research, National University of Ireland Maynooth, Ireland (e-mail: giorgio.bacelli@eng.nuim.ie).*
** *Center for Ocean Energy Research, National University of Ireland Maynooth, Ireland (e-mail: john.ringwood@eeng.nuim.ie).*

Abstract: Wave energy converters (WECs) require active control to maximise energy capture over a wide range of sea conditions, which is generally achieved by making the device resonate. The exaggerated device motion arising at resonance, however, may result in nonlinear effects that are ignored by the linear models that are typically employed. In particular, nonlinear viscous forces are significant for particular device types, such as hinged flaps, which we take as a case study in this paper. The paper develops a general nonlinear WEC control methodology based on pseudospectral methods. The continuous time energy maximization problem is fully discretised (both state and control), and the optimal solution is obtained by solving the resulting finite dimensional optimization problem. By way of example, the nonlinear viscous damping for a hinged flap WEC is incorporate into the control model. It is shown that the ratio of energy captured to energy dissipated is significantly increased with the nonlinear controller, compared to the linear case.

1. INTRODUCTION

Wave energy conversion is the process of transforming energy carried by water waves in the sea into a usable form of energy, e.g. electricity. Devices designed to fulfil this task are known as Wave Energy Converters (WECs), and this paper concerns the control of a particular type of device, where the objective of the control system is to maximise the amount of energy absorbed. The device considered in this paper is a bottom-hinged vertical plate (Fig. 1) which which exploits the same conversion principle as the *Oyster* WEC being developed by *Aquamarine power Ltd.* (Folley et al., 2007). The force exerted by the incident waves (excitation force) induces a pitching motion on the plate. Part of the mechanical work done by the excitation force is converted into a usable form of energy by means of the Power Take Off (PTO), a component of the WEC capable of doing mechanical work on the oscillating plate by exerting a force, which is the control variable.

Most studies, academic and commercial, focus on the use of linear models; their appeal is mainly due to the possibility of developing analytical solutions for the control problems and analysis of performance (Falnes, 2002). A variety of sources introduce nonlinearities in the model of WECs, from the PTO (Engja and Hals, 2007; Bacelli et al., 2008) to the fluid-body interactions. While it is reasonable to assume a linear approximation for the radiation (Gilloteaux, 2007), some studies have shown the wide disparity between linear and nonlinear models of excitation forces (Merigaud et al., 2012), viscous forces (Folley et al., 2007) and hydrostatic restoring forces (Zurkinden and Kramer, 2012). This paper focusses on viscous drag applied to a hinged flap WEC as an example to illustrate the application of the pseudospectral methods for the nonlinear control of wave energy converters. However, the nonlinear control framework is general and can be applied to other nonlinearities and WEC device types.

The control problem is an optimal control problem because the objective is to find value of the control (PTO force) which maximises the amount of absorbed energy. In this paper, the solution to the nonlinear optimal control of a WEC is obtained by means of pseudospectral methods, which are a subset of the class of techniques used for the discretisation of integral and partial differential equations known as mean weighted residuals (Fornberg, 1996; Canuto et al., 2006). The first applications of pseudospectral optimal control has been presented more than fifteen years ago (Elnagar et al., 1995; Vlassenbroeck and Van Dooren, 1988); however, only in recent years has it received increasing attention (Garg et al., 2010; Ross and Karpenko, 2012) and found application, mostly in flight control.

Previous approaches to nonlinear control of WECs include the application of Pontryagin's maximum principle to the continuous time optimal control problem (Babarit and Clément, 2006; Nielsen et al., 2013) and its discretisation (Tom and Yeung, 2013; Richter et al., 2013). However, discretisation using pseudospectral methods generally gives a faster convergence rate (Benson, 2005), which results in a smaller nonlinear program and reduced computing time, thus suitable for real-time applications. Additionally, the discretisation by means of the pseudospectral method presented in this paper allows the convolution integral that models the radiation force to be simplified analytically,

⋆ This work was supported by Enterprise Ireland under contract TD/2009/0331.

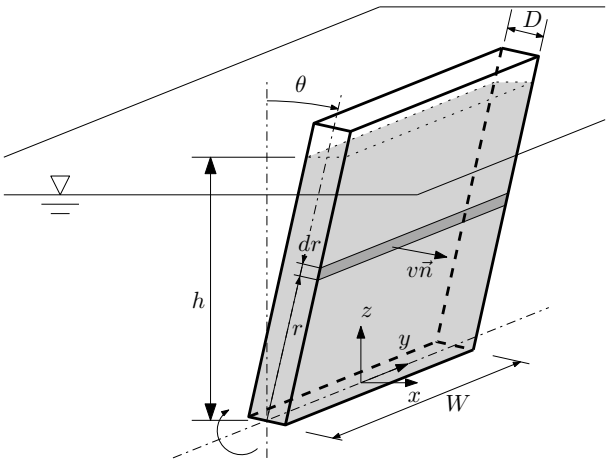

Fig. 1. Flap-type wave energy converter. The shaded area indicates the submerged region.

instead of the classical approach of using system identification to build a state space model (Tom and Yeung, 2013) or being completely neglected (Richter et al., 2013).

The remainder of the paper is organised as follow: the dynamical model of the flap-type WEC is described in Sec. 2, and a brief overview of pseudospectral optimal control is provided in Sec. 3, while Sec. 4 shows a case study for the flap-type device. Simulation results are illustrated and discussed in Sec. 5, with conclusions drawn in Sec. 6.

2. WEC DYNAMICAL MODEL

The device considered in this paper is depicted in Fig. 1. It is a flap-type WEC hinged on the y axis at a depth h=15m, with a width W=30m, thickness D=1m and a uniform density ρ_b= 250kg/m^3. The equation of motion is derived from Euler's second law, which says that the rate of change of the angular momentum is equal to the sum of the external moments of force about the axis y:

$$I_y\,\ddot{\theta} = \gamma_w(t) + \gamma_p(t).$$

I_y is the moment of inertia of the body with respect to the axis y, γ_p is the torque applied by the PTO, and γ_w is the resultant of the moments due to the interaction between water and the oscillating body, which is composed of four terms, as described by Folley et al. (2007):

$$\gamma_w(t) = \gamma_h(t) + \gamma_d(t) + \gamma_r(t) + \gamma_e(t).$$

The hydrostatic restoring moment γ_h is assumed to be linearly proportional to the pitch angle ($\gamma_h = S_h\,\theta$), where S_h is the hydrostatic restoring coefficient. The excitation torque γ_e is due to the effect of the incident waves, and is calculated as $\gamma_e(t) = h_e * \zeta$, where ζ is the wave elevation and $*$ denotes the convolution operator

$$f * g = \int_{-\infty}^{-\infty} f(t-\tau)g(\tau)d\tau.$$

The radiation torque γ_r is due to the motion of the body which causes waves to be radiated away, and it depends on the velocity and acceleration of the oscillating body as (Cummins, 1962):

$$\gamma_r = -I_\infty\,\ddot{\theta} - h_r * \dot{\theta}$$

The functions h_e and h_r are, respectively, the impulse responses of the excitation and radiation, while I_∞ is known as the asymptotic value of the added inertia for "infinite frequency" (Falnes, 2002). The values of h_e, h_r and I_∞ were calculated by means of the boundary element software WAMIT (2013).

The nonlinear part of the dynamic model is due to the moment of the drag force (f_d), which is generally modelled as proportional to the square of the fluid velocity normal to the surface of the body (Journée and Massie, 2001):

$$f_d = -(1/2)\rho C_d A v|v|,$$

where ρ is the density of the water, C_d is the drag coefficient, A is the area normal to the direction of the relative fluid flow and v is the velocity normal to the surface (Fig. 1). When the body is in the vertical position ($\theta = 0$), for small oscillations, the normal velocity on the vertical surface is related to the angular velocity as $v \approx r\dot{\theta}$, where r is the vertical distance between the hinge and the point of the surface where the velocity is considered. The contribution to the drag force of the infinitesimal surface at distance r from the hinge, of width W and height dr (Fig. 1) is $df_d \approx -(1/2)\rho C_d W r^2\dot{\theta}|\dot{\theta}|dr$. The infinitesimal moment of the drag force applied with respect to the axis y is $d\gamma_v = r\,df_d$; by integrating $d\gamma_v$ from 0 to h, the total moment of the drag force applied to the hinge is:

$$\gamma_v = -\frac{1}{2}\int_0^h \rho C_d W r^3\dot{\theta}|\dot{\theta}|dr = -B_v\,\dot{\theta}|\dot{\theta}|$$

where $B_v = (1/8)\rho\,C_d W h^4$. According to Blevins (1992), the drag coefficient of a plate orthogonal to the direction of the flow is $C_d = 1.9$ (Blevins, 1992). The resulting equation of motion is

$$I_t\,\ddot{\theta} = -B_{v_1}\dot{\theta} - B_{v_2}\dot{\theta}|\dot{\theta}| - h_r * \dot{\theta} - S_h\,\theta + \gamma_p + \gamma_e. \quad (1)$$

where $I_t = (I_y + I_\infty)$, and B_{v_1} is the coefficient of a linear dissipative term, which models additional losses occurring at small velocities, when the effect of the quadratic term is negligible (Journée and Massie, 2001).

3. PSEUDOSPECTRAL OPTIMAL CONTROL

Pseudospectral optimal control is a method for the direct transcription of an optimal control problem (Ross and Karpenko, 2012), which means that both control and state variables are discretised, and the original control problem is approximated by a nonlinear program.

Consider, for example, the optimal control problem: determine the control $\boldsymbol{u}(t) \in \mathbb{R}^m$, that minimises, or maximises, the cost functional in the Lagrange form (Stengel, 1986):

$$J = \int_0^T g(\boldsymbol{x}, \boldsymbol{u}, t)\,dt, \qquad g : \mathbb{R}^n \times \mathbb{R}^m \times \mathbb{R} \to \mathbb{R} \quad (2)$$

subject to the dynamic constraint

$$\dot{\boldsymbol{x}} = \boldsymbol{f}(\boldsymbol{x}, \boldsymbol{u}, t) \quad t \in [0, T], \quad (3)$$

where $\boldsymbol{x}(t) \in \mathbb{R}^n$ and $\boldsymbol{f} : \mathbb{R}^n \times \mathbb{R}^m \times \mathbb{R} \to \mathbb{R}^n$.

The first step is to approximate the state and control variables by considering, for the i-th components, the following expansion:

$$x_i(t) \approx x_i^N(t) := \sum_{k=1}^{N} \hat{x}_{ik}\phi_k(t) = \Phi(t)\hat{\boldsymbol{x}}_i \tag{4}$$

$$u_i(t) \approx u_i^N(t) := \sum_{k=1}^{N} \hat{u}_{ik}\phi_k(t) = \Phi(t)\hat{\boldsymbol{u}}_i \tag{5}$$

where

$$\hat{\boldsymbol{x}}_i = [\hat{x}_{i1}, \hat{x}_{i2}, \ldots, \hat{x}_{iN}]^T,$$
$$\hat{\boldsymbol{u}}_i = [\hat{u}_{i1}, \hat{u}_{i2}, \ldots, \hat{u}_{iN}]^T,$$

and

$$\Phi(t) = [\phi_1(t), \phi_2(t), \ldots, \phi_N(t)]$$

form a basis for an N-dimensional vector space, on which the state and control variables are approximated. It is also convenient to define the vectors $\boldsymbol{X} \in \mathbb{R}^{Nn}$ and $\boldsymbol{U} \in \mathbb{R}^{Nm}$:

$$\boldsymbol{X} = \left[\hat{\boldsymbol{x}}_1^T, \ldots, \hat{\boldsymbol{x}}_n^T\right]^T \qquad \boldsymbol{U} = \left[\hat{\boldsymbol{u}}_1^T, \ldots, \hat{\boldsymbol{u}}_n^T\right]^T.$$

As the result of the approximations, the cost functional (2) depends only on the $N(n+m)$ coefficients in $\boldsymbol{X}$ and $\boldsymbol{U}$, thus the optimisation problem is finite dimensional.

To illustrate the effect of the approximation on the dynamic equation, the derivative of the approximated state variable is considered first, that is:

$$\dot{x}_i^N = \sum_{k=1}^{N} \hat{x}_{ik}\dot{\phi}_k(t) = \dot{\Phi}(t)\hat{\boldsymbol{x}}_i. \tag{6}$$

By substituting (4), (5) and (6) into (3), the approximated dynamic equation in the residual form is then

$$r_i(t) = \dot{x}_i^N(t) - f_i(\boldsymbol{x}^N(t), \boldsymbol{u}^N(t), t), \quad i = 1, \ldots, n \tag{7}$$

where $\boldsymbol{x}^N$ and $\boldsymbol{u}^N$ are, respectively, the vectors of the approximated state variables and control variables, the elements of which are x_i^N defined in (4) and u_i^N defined in (5). The coefficients $\hat{\boldsymbol{x}}_i$ and $\hat{\boldsymbol{u}}_j$ for which the n residuals (7) are minimised are calculated by using the pseudospectralpectral method (Elnagar et al., 1995), also known as *collocation* method. The method consists of collocating the system dynamics at a number of time points t_k, called *nodes*, meaning that the coefficients $\hat{\boldsymbol{x}}_i$ and $\hat{\boldsymbol{u}}_j$ are such that the dynamic equation is satisfied at a number of points t_k, or equivalently, the residuals r_i are zero at the N_c nodes:

$$r_i(t_j) = \dot{\Phi}(t_j)\hat{\boldsymbol{x}}_i - f_i\left(\boldsymbol{X}, \boldsymbol{U}, t_j\right) = 0 \tag{8}$$

which is a system of $n \times N_c$ equations because $j = 1, \ldots, N_c$ and $i = 1, \ldots, n$.

The functional J in (2) is also approximated by an appropriate quadrature formula with weights w_j, as

$$J^N = \int_0^T g(\boldsymbol{X}, \boldsymbol{U}, t)\, dt \approx \sum_{j=0}^{N_c} g(\boldsymbol{X}, \boldsymbol{U}, t_j) w_j, \tag{9}$$

and the optimal control problem defined by the cost functional (2) and the dynamic constraint (3) is transformed into the finite dimensional optimisation problem: find $\boldsymbol{U}$ and $\boldsymbol{X}$ to maximise (or minimise) (9) subject to the constraints (8).

The collocation of the dynamic equation and of the cost functional, that is the choice of the nodes t_j, depend on a number of factors, among which the expansions (4) and (5) (Ross and Karpenko, 2012; Garg et al., 2010)

4. OPTIMAL WEC CONTROL

The optimal control problem that we are aiming to solve is the maximisation of the absorbed energy, which is equivalent to maximising the amount of work done by the PTO moment

$$J = \int_0^T \gamma_p(t)\, \dot{\theta}(t)\, dt, \tag{10}$$

subject to the constraint given by the dynamic model in (1). The first step is to choose the expansion for the state and control and, given the oscillatory nature of the problem, a zero-mean trigonometric polynomial (truncated Fourier series) is a sensible choice, thus:

$$x_i(t) \approx \sum_{k=1}^{N/2} x_{ik}^c \cos(k\omega_0 t) + x_{ik}^s \sin(k\omega_0 t) = \Phi(t)\hat{\boldsymbol{x}}_i \tag{11}$$

$$u(t) \approx \sum_{k=1}^{N/2} u_k^c \cos(k\omega_0 t) + u_k^s \sin(k\omega_0 t) = \Phi(t)\hat{\boldsymbol{u}} \tag{12}$$

where

$$\hat{\boldsymbol{x}}_i = \left[x_{i1}^c, x_{i1}^s, \ldots, x_{i\frac{N}{2}}^c + x_{i\frac{N}{2}}^s\right]^T$$
$$\hat{\boldsymbol{u}} = \left[u_1^c, u_1^s, \ldots, u_{\frac{N}{2}}^c + u_{\frac{N}{2}}^s\right]^T$$
$$\Phi(t) = \left[\cos(\omega_0 t), \sin(\omega_0 t), \ldots, \cos\left(\frac{N}{2}\omega_0 t\right), \sin\left(\frac{N}{2}\omega_0 t\right)\right]$$

and the fundamental frequency is $\omega_0 = 2\pi/T$.

By substituting the state (11) and control (12) expansions into the cost function (10), the approximated absorbed energy is

$$J^N = \int_0^T \hat{\boldsymbol{u}}^T \Phi^T(t)\, \Phi(t)\hat{\boldsymbol{x}}_2\, dt = \frac{T}{2}\hat{\boldsymbol{u}}^T\hat{\boldsymbol{x}}_2, \tag{13}$$

because of the orthogonality of the basis Φ, that is $\langle\phi_i, \phi_j\rangle = \delta_{ij}T/2$, where δ_{ij} is the Kronecker delta.

The derivative of the state variables in (6), given the approximation of the state in (11), becomes

$$\dot{x}_i^N = \dot{\Phi}(t)\hat{\boldsymbol{x}}_i = \Phi(t)\, \mathrm{D}_\phi\, \hat{\boldsymbol{x}}_i \tag{14}$$

where $\mathrm{D}_\phi \in \mathbb{R}^{N\times N}$ is a block diagonal matrix, with the k-th block is defined as

$$\mathrm{D}_\phi^k = \begin{bmatrix} 0 & k\,\omega_0 \\ -k\,\omega_0 & 0 \end{bmatrix}.$$

The state vector is composed of the angular position and velocity, that is, $\boldsymbol{x} = [x_1, x_2]^T = [\theta, \dot{\theta}]^T$, and the control input is the PTO moment ($u = \gamma_p$), thus $n = 2$ and $m = 1$. Consequently, the dynamic equation (1) can be transformed into the system of equations:

$$\dot{x}_1 = x_2 \tag{15}$$

$$I_t\, \dot{x}_2 = -B_{v_1} x_2 - B_{v_2} x_2 |x_2| - h_r * x_2 - S_h x_1 + u - \gamma_e \tag{16}$$

By applying the approximations (11) and (14) to the first state equation (15), the result is

$$\Phi(t)\, \mathrm{D}_\phi\, \hat{\boldsymbol{x}}_1 - \Phi(t)\, \hat{\boldsymbol{x}}_2 = 0 \quad \Leftrightarrow \quad \mathrm{D}_\phi\, \hat{\boldsymbol{x}}_1 - \hat{\boldsymbol{x}}_2 = 0. \tag{17}$$

because the elements of Φ form basis.

The residuals of the second state equation (16), collocated at the nodes t_j are

$$r_j = \mathrm{I}_t\,\Phi_j\,\mathrm{D}_\phi\,\hat{\boldsymbol{x}}_2 + B_{v_1}\Phi_j\,\hat{\boldsymbol{x}}_2 + B_{v_2}\Phi_j\,\hat{\boldsymbol{x}}_2|\Phi_j\,\hat{\boldsymbol{x}}_2| + S_h\Phi_j\,\hat{\boldsymbol{x}}_1 + (h_r * \Phi)_{t_j}\,\hat{\boldsymbol{x}}_2 - \Phi_j\,\hat{\boldsymbol{u}} - \gamma_e(t_j). \quad (18)$$

where $\Phi_j = \Phi(t_j)$. The convolution term can be simplified by substituting the approximation (11) into the convolution integral; after some basic derivations involving trigonometric identities and the definition of the sine and cosine transforms, which we omit for brevity, the result is

$$(h_r * \Phi)_{t_j}\,\hat{\boldsymbol{x}}_2 = \int_{-\infty}^{+\infty} h_r(t_j - \tau)\,x_2^N(\tau)\,d\tau \quad (19)$$

$$= \Phi_j\,(\mathrm{G} - I_\infty \mathrm{D}_\Phi)\,\hat{\boldsymbol{x}}_2, \quad (20)$$

where the matrix $\mathrm{G} \in \mathbb{R}^{N\times N}$ is block diagonal, and the k-th block is

$$\mathrm{G}_k = \begin{bmatrix} B(k\,\omega_0) & k\,\omega_0 A(k\,\omega_0) \\ -k\,\omega_0 A(k\,\omega_0) & B(k\,\omega_0) \end{bmatrix}.$$

The frequency domain coefficients A and B are related to the impulse responses by means of the Cummins relations (Cummins, 1962), and they are provided directly by WAMIT (2013).

Substituting (20) into (18), the residuals simplify to

$$r_j = I_y\Phi_j\,\mathrm{D}_\phi\,\hat{\boldsymbol{x}}_2 + B_{v_1}\Phi_j\,\hat{\boldsymbol{x}}_2 + B_{v_2}\Phi_k\,\hat{\boldsymbol{x}}_2|\Phi_j\,\hat{\boldsymbol{x}}_2| + \Phi_j\,\mathrm{G}\,\hat{\boldsymbol{x}}_2 + S_h\Phi_j\,\hat{\boldsymbol{x}}_1 - \Phi_j\,\hat{\boldsymbol{u}} - \gamma_e(t_j) = 0. \quad (21)$$

The nodes t_j are uniformly spaced between 0 and $T - \Delta t$:

$$t_j = j\,\Delta t, \quad \text{with } \Delta t = T/(N+1) \quad \text{and } j = 0, \ldots, N.$$

The vectors $\boldsymbol{U}$ and $\boldsymbol{X}$, that give the optimal profile for the PTO moment and the motion of the flap, respectively, are the solutions of the nonlinear program which maximises the absorbed energy (13), subject to the $2N$ equality constraints due to the dynamic equations (17) and (21).

5. RESULTS

Simulations have been carried out in Matlab and the algorithm used for solving the optimisation problem is the Sequential Quadratic Programming implemented by the *fmincon* function included in the Optimization Toolbox.

Figure 2 presents simulation results for an incident wave of amplitude $|\zeta|$=2m and period T=10s, where the state variables $(\theta, \dot{\theta})$ and the control input (γ_p) have been approximated using seven frequency components each (N=14). Figure 2a clearly shows that the controller aims to limit the angular velocity of the device, as the time profile of $\dot{\theta}$ resembles a "flattened" sinusoid and time profile of the angular position seems to approach a motion at constant speed in the time intervals $t \in [1.5, 4]$ and $t \in [6, 8.5]$. The PTO and the excitation moments are depicted in Fig. 2b while the instantaneous absorbed power is in Fig. 2c. Comparison of Fig. 2a and 2b also shows that the controller tries to keep the velocity in phase with the excitation, as in happens in the linear case (Falnes, 2002).

Figure 3 shows the frequency contents of the state and control variables, in addition to the absorbed power. The amplitude of the frequency components decay quickly as the frequency increases, meaning that only a few components are necessary for a good approximation. This is confirmed by looking at Table 1, where the average absorbed power (P_u), defined as

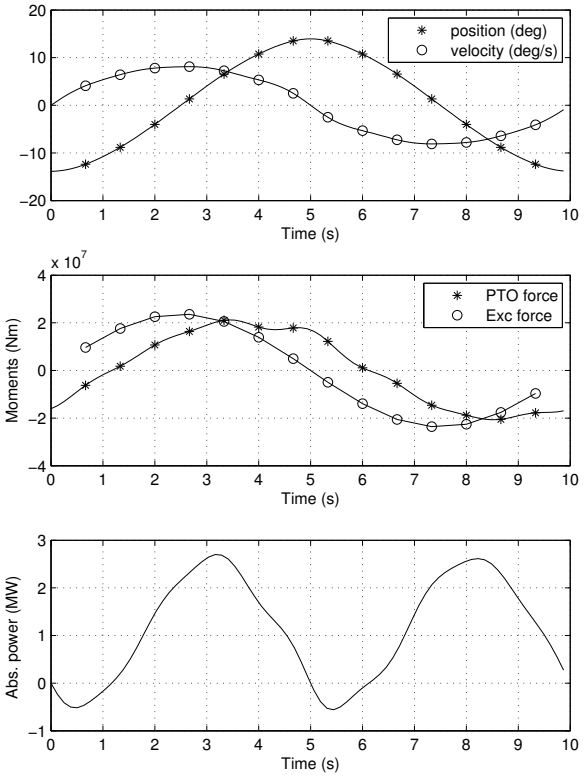

Fig. 2. Motion, forces and absorbed power for $T = 10s$, $\zeta_a = 2m$ and for $N = 14$.

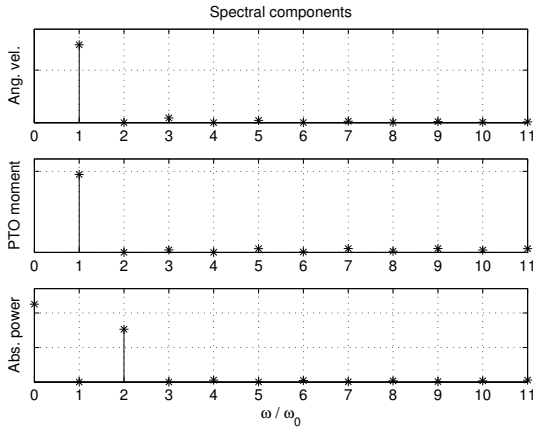

Fig. 3. Spectral components of the velocity, the PTO moment and the absorbed power for $T = 10s$ and $\zeta_a = 2m$

$$P_u = \frac{1}{T}J^N = \frac{1}{2}\hat{\boldsymbol{u}}^T\hat{\boldsymbol{x}},$$

is listed for different values of the expansion order N, and for different values of the wave period. The computation times of the optimisation problems, using a laptop computer with a Core i7 processor working at $2.8GHz$ are listed in brackets. Based on the results given in Table 1, the value of $N = 10$ has been used for the simulations presented in the rest of this paper as the best trade-off between speed and accuracy. Thus, position, velocity and

PTO force are each approximated with a trigonometric polynomial with five frequency components, and the resulting approximate optimal control problem is a nonlinear program with 30 variables and 20 constraints.

In Fig. 4, the average absorbed power is depicted as function of the wave period and wave amplitude. It is interesting to note that, with the model including a quadratic viscous damping term, the absorbed power increases with $|\zeta|^{\frac{3}{2}}$ rather than $|\zeta|^2$, as in the linear case (Falnes, 2002). This fact is highlighted in Fig. 5, where the solid curve is the absorbed power as function of the wave amplitude $|\zeta|$, when only the linear dissipative term is present ($B_{v_2} = 0$); in this case, P_u is proportional to the square of the wave amplitude ($P_u \propto |\zeta|^2$). The dashed curve is the absorbed power when the nonlinear term is also included ($B_{v_1} \neq 0, B_{v_2} = 0$), and P_u increases with the wave amplitude as $P_u \propto |\zeta|^{\frac{3}{2}}$.

Of particular interest is Fig. 6, which depicts the ratio of the average absorbed power over the sum of the power radiated and the power dissipated by the linear and quadratic terms, P_u/P_d, where

$$P_d = \frac{1}{T}\int_0^T \left(B_{v_1}\dot{\theta} + B_{v_2}\dot{\theta}|\dot{\theta}| + h_r * \dot{\theta}\right)\dot{\theta}dt.$$

Note that the ratio P_u/P_d is always greater than one, which is the value of P_u/P_d when the model is linear (Falnes, 2002). This fact does not imply that more energy is being absorbed, but only that a larger fraction of the total power flowing through the device is being converted, as the overall absorbed power is smaller because it increases with $|\zeta|^{\frac{3}{2}}$. This result is consistent with the linear absorption theory; in fact, when the amplitude of the incident wave is small, the linear dissipative term is dominant with respect to the quadratic term, and the ratio $P_u/P_d \to 1$, which is what happens in the linear case. The ratio P_u/P_d becomes close to 1 also when the wave period is close to $T = 5s$, for which the linear radiation damping B becomes the dominant term (Fig. 7).

An additional significant difference with the linear case can be observed in Fig.8, which depicts the ratio of the reactive power over the absorbed power, where the average reactive power is defined as the power that the PTO returns to the oscillating body:

$$P_{reac} = -\frac{1}{T}\int_0^T \min\left[P(t), 0\right] dt, \text{ where } \quad P(t) = \dot{\theta}\,\gamma_p.$$

The ratio P_{reac}/P_u is generally small for the range of wave periods and amplitudes considered, when the quadratic term becomes dominant, which is a favourable characteristic when designing a wave energy converter, because PTOs that are unable to return power to the oscillating body are generally less expensive. The consistency with the linear model can also be observed from the results in this figure (Fig.8) when considering small wave amplitudes, where the amount of reactive power compared to the absorbed power increases considerably. It is well known that, with an optimal linear controller, the amount of reactive power is large when the period of the incident wave is far away from the resonance period (Falnes, 2002).

Table 1. Absorbed energy (kW) and computing time (in brackets), as function of the order of the approximation (N) and of the wave period (T) for a wave amplitude of $|\zeta| = 2m$.

N	T=4s	T=8s	T=14s	T=20s
6	563.7 (0.16)	1463 (0.19)	685.5 (0.14)	399.8 (0.18)
10	564.5 (0.43)	1472 (0.31)	687.5 (0.32)	401.5 (0.37)
14	654.6 (0.89)	1473 (0.64)	687.7 (0.58)	401.6 (0.56)
18		1473 (1.17)	687.7 (0.98)	401.6 (0.79)

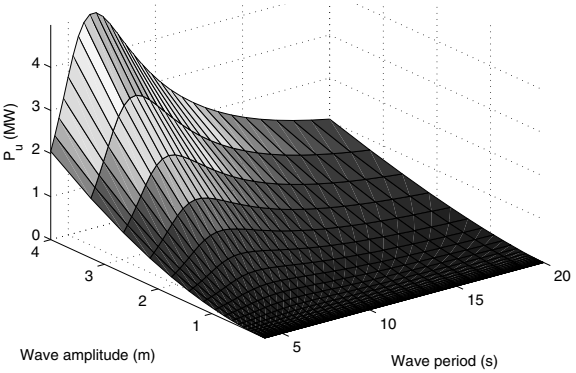

Fig. 4. Average absorbed power (P_u).

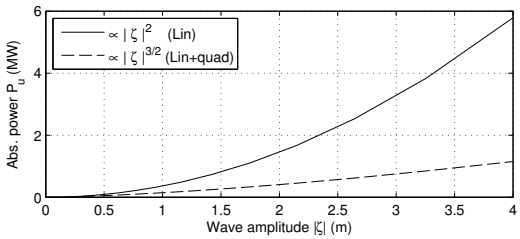

Fig. 5. Absorbed power as function of the wave amplitude for the linear and nonlinear models (T=20s).

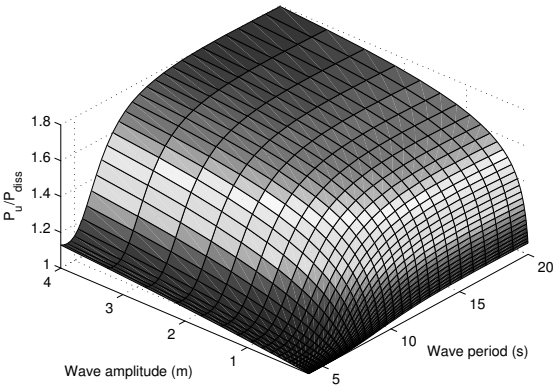

Fig. 6. Ratio of the average absorbed power (P_u) over the dissipated and radiated power

6. CONCLUSION

This paper presents a nonlinear WEC control framework using pseudospectral methods, which are known for their convergence properties, in the sense that few coefficients are required for obtaining a good approximation, confirmed by the data in Table 1. The consequence is that

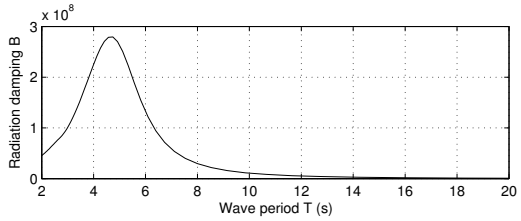

Fig. 7. Radiation damping B.

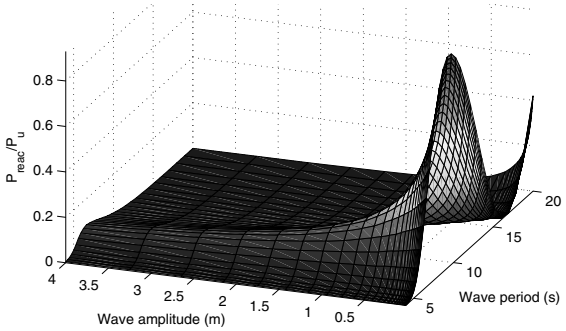

Fig. 8. Ratio of the average reactive power over the average absorbed power

the dimension of the nonlinear program and its computing time are small, thus the technique is a good candidate for being implemented in real time applications.

Analysis of results for monochromatic waves at different frequencies and amplitudes show significant differences with linear theory. In particular the optimal nonlinear controller provides better ratio between the average absorbed power and dissipated power, when the effect of the nonlinear terms are predominant. This is the case for the hinged flap device which provides the application example. Additionally, the optimal nonlinear control law requires the PTO to return a smaller fraction of reactive power to the oscillating body compared to the optimal linear control law, placing less demands on the PTO system. In addition, more cost effective and reliable PTO configurations, such as hydraulic PTOs, which are not well suited for the implementation of the linear control law, due to their strong nonlinearities (Bacelli et al., 2008), can be employed.

ACKNOWLEDGEMENTS

The authors would like to thank Dr. Ronan Costello and Thomas Kelly for their support provided on the numerical modelling.

REFERENCES

A. Babarit and A. Clément. Optimal latching control of a wave energy device in regular and irregular waves. *Applied Ocean Research*, 28(2):77–91, April 2006.

G. Bacelli, J.-C. Gilloteaux, and R. J. V. State space model of a hydraulic power take off unit for wave energy conversion employing bondgraphs. In *Proc. 10th World Renewable Energy Congress - WRECX, Glasgow*, 2008.

D. A. Benson. *A Gauss pseudospectral transcription for optimal control*. PhD thesis, Massachusetts Institute Of Technology, 2005.

R. Blevins. *Applied Fluid Dynamics Handbook*. Krieger Publishing Company, 1992.

C. Canuto, Y. Hussaini, A. Quarteroni, and T. Zang. *Spectral Methods: Fundamentals in Single Domains*. Springer, 2006.

W. Cummins. The impulse response function and ship motions. *Schiffstechnik*, 9:101–109, 1962.

G. Elnagar, M. Kazemi, and M. Razzaghi. The pseudospectral legendre method for discretizing optimal control problems. *IEEE Transactions on Automatic Control*, 40:1793–1796, 1995.

H. Engja and J. Hals. Modelling and simulation of sea wave power conversion systems. In *Proc. 7th European Wave and Tidal Energy Conference, EWTEC*, September 2007.

J. Falnes. *Ocean waves and oscillating systems: linear interactions including wave-energy extraction*. Cambridge University Press, 2002.

M. Folley, T. Whittaker, and J. van't Hoff. The design of small seabed-mounted bottom-hinged wave energy converters. In *Proc. of 7th European Wave and Tidal Energy Conference, EWTEC*, Porto, 2007.

B. Fornberg. *A Practical Guide to Pseudospectral Methods*. Cambridge University Press, 1996.

D. Garg, M. Patterson, W. W. Hager, A. V. Rao, D. A. Benson, and G. T. Huntington. A unified framework for the numerical solution of optimal control problems using pseudospectral methods. *Automatica*, 46(11):1843 – 1851, 2010.

J.-C. Gilloteaux. *Mouvements de grande amplitude d'un corps flottant en fluide parfait. Application à la récupération de l'énergie des vagues*. PhD thesis, Ecole Centrale de Nantes, France, 2007.

J. Journée and W. Massie. *Offshore Hydromechanics*. Delft University of Technologyy, 2001.

A. Merigaud, J.-C. Gilloteaux, and R. J. V. A nonlinear extension for linear boundary element methods in wave energy device modelling. In *Proc. of 31st International Conference on Ocean, Offshore and Arctic Engineering (OMAE2012)*, 2012.

S. Nielsen, Q. Zhou, M. Kramer, B. Basu, and Z. Zhang. Optimal control of nonlinear wave energy point converters. *Ocean Engineering*, 72(0):176 – 187, 2013.

M. Richter, M. Magana, O. Sawodny, and T. Brekken. Nonlinear model predictive control of a point absorber wave energy converter. *Sustainable Energy, IEEE Transactions on*, 4(1):118–126, January 2013.

I. M. Ross and M. Karpenko. A review of pseudospectral optimal control: From theory to flight. *Annual Reviews in Control*, 36(2):182 – 197, 2012.

R. Stengel. *Optimal Control and Estimation*. Dover books on advanced mathematics. Dover Publications, 1986.

N. Tom and R. W. Yeung. Non-linear model predictive control applied to a generic ocean-wave energy extractor. In *Proc. of 32nd International Conference on Ocean, Offshore and Arctic Engineering (OMAE)*, 2013.

J. Vlassenbroeck and R. Van Dooren. A Chebyshev technique for solving nonlinear optimal control problems. *Automatic Control, IEEE Transactions on*, 33(4):333–340, 1988.

WAMIT. *WAMIT Inc. USA*, 2013. URL `www.wamit.com`.

A. S. Zurkinden and M. Kramer. Numerical time integration methods for a point absorber wave energy converter. In *Proc. of 27th International Workshop on Water Waves and Floating Bodies, Copenhagen*, 2012.